Article

Journal of Vibration and Control
2018, Vol. 24(18) 4096–4109

DOI: 10.1177/1077546317719194
journals.sagepub.com/home/jvc
SAGE

On the vibration analysis of power lines with moving dampers

MA Bukhari[1], O Barry[1] and E Tanbour[2]

Abstract

This work investigates the performance of a moving damper for overhead transmission lines. The damper or absorber consists of mass-spring-damper-mass system. The absorber is connected to a single conductor subjected to pretension and wind force. The governing equations of motion are obtained using Hamilton's principle, and numerical analysis is carried out using MATLAB®. The model is validated by comparing the present results to those in the literature. Parametric studies are conducted to investigate the performance of the proposed absorber. The results indicate that a moving absorber can be more effective than a fixed absorber. It is also demonstrated that the vibration displacement decreases with increasing forcing frequency and decreasing absorber speed.

Keywords

Power lines, Stockbridge Damper, moving absorber, mass-spring-damper-mass, aluminum conductor steel reinforced

1. Introduction

Aeolian vibration of overhead transmission lines has been a subject of study for many years. The development of repetitive cycle motions resulting from the wind force can cause tremendous damage to power networks. This type of wind-induced motion is specific to single conductor, and it is characterized by low amplitudes and high frequency vibration. The frequency of Aeolian vibration ranges from 3 to 150 Hz while the wind speed ranges from 1 to 7 m/s (Barry et al., 2013, 2014c, 2015b; EPRI, 2006). The amplitude of vibration is usually less than the diameter of the conductor.

Aluminum conductor steel reinforced is the most common conductor utilized in overhead transmission lines. It consists of aluminum outer layers and steel inner layers. The outer layers are for electric power transmission and the inner layers are for strength required to support the weight of the cable without straining the aluminum. The conductor diameter ranges from 6 to 50 mm.

When vibration is left uncontrolled, it causes fatigue failure at the point of contact between the cable and the suspension clamps. Aeolian vibration is usually controlled by attaching Stockbridge dampers or reducing the cable tension (Oliveira and Preire, 1994). The role of the damper is to reduce the vibration amplitude to a safe level. The reduction of tension also minimizes the vibration level.

Numerous authors have examined vibration of transmission lines by using the energy balance method (Kraus and Hagerdorn, 1991; Oliveira and Preire, 1994; Shafer, 1984; Verma and Hagerdorn, 2005) and the method of impedance (Nigol et al., 1985; Rawlins, 1958; Tompkins et al., 1956). An attempt to depart from the energy balance method is reported (Barry et al., 2014c, 2016). Both conductor and Stockbridge dampers are modeled as Euler–Bernoulli beams in Barry et al. (2014c) while in Barry et al. (2016) only the conductor is modeled as a beam. The Stockbridge damper is reduced to a mass-spring-damper-mass system. In Barry et al. (2014c) and Barry et al. (2016), it was demonstrated that the efficiency of Stockbridge dampers is characterized by the number of resonant frequencies they possess and their location on the conductor. In fact, Stockbridge dampers were found to be inefficient when their locations coincide with a vibration node. Hence, there is a need for replacing the static

[1]College of Science and Engineering, Central Michigan University, Mount Pleasant, MI, USA 48859
[2]College of Technology, Eastern Michigan University, Ypsilanti, MI, USA 48197

Received: 4 December 2016; accepted: 7 June 2017

Corresponding author:
O Barry, College of Science and Engineering, Central Michigan University, Mount Pleasant, MI 48859, USA.
Email: barry1o@cmich.edu

Stockbridge damper with a dynamic damper. This will allow significant vibration attenuation of the conductor at any forcing frequency provided that the dynamic damper is capable of positioning itself at an antinode at any time. Recently, Barry et al (2015a), disclosed a mobile damper mechanism capable of positioning itself at an antinode at any time. The disclosed mobile damper is patent pending.

The vibration of a beam with moving or fixed absorber consisting of a mass or spring-damper-mass systems has been investigated by numerous authors (Chang et al., 2006; Gašić et al., 2011; Jacksic et al., 2014; Majumder and Manohar, 2002; Oguamanam and Hansen, 1998; Pesterev and Bergman, 2000; Pesterev et al., 2001, 2003; Stăncioiu et al, 2008; Yang, et al., 2000) and (Barry et al., 2014a, 2014b; Alkhaldi et al., 2013, 2013; Samani and Pellicano, 2009, 2012; Samani et al., 2013; Snowdon, 1965; Song et al., 2016; Wu, 2006), respectively. However, no work has been reported for the combination of a beam under tensile load with a dynamic absorber consisting of an in-span mass connected to a small suspended mass through a spring-damper system. The present paper examines this system. It is an extension of Barry et al. (2016), in that the conductor is modeled as a beam subjected to a tensile force while the Stockbridge damper is modeled as a moving mass-spring-damper-mass system. The whole system (i.e., beam under a tensile load with a dynamic absorber) is subjected to a wind force.

2. System description

Figure 1(a) illustrates a schematic diagram for a Stockbridge damper attached to a single conductor with length of L, a flexural rigidity of EI, and mass per unit length m. The Stockbridge damper consists of an in-span mass m_c (clamp) and a messenger or (damper cable) which is fixed to the bottom edge of the clamp. At each end of the messenger, there is a mass or counterweight (m_{dl} and m_{dr}). Each mass with its messenger can be modeled as a cantilever Euler–Bernoulli beam with mass at each end, as shown in Figure 1(b). The two cantilever beams can further be reduced to an equivalent single degree of freedom system, which has equivalent mass m_a, equivalent stiffness k, and equivalent damping coefficient c, as shown in Figure 1(c). The Stockbridge damper is usually installed at 2–5 m from the tower. This distance represents around 1–2% of the total length of the conductor. At this distance, the damper may work effectively for a specific excitation frequency provided that the location of the absorber does not coincide with a node. However, the span length of the conductor in transmission lines is very long; it is impossible for a fixed absorber to cover a wider range of frequencies. The proposed absorber can be installed on transmission lines as a Stockbridge damper with wheels and driving motor in replacement of the clamp. Other mechanisms that are used in moving robots for power transmission lines inspection can also be employed as a possible way to move the absorber along the conductor (Li and Ruan, 2010; Park et al., 2012; Wang et al., 2010).

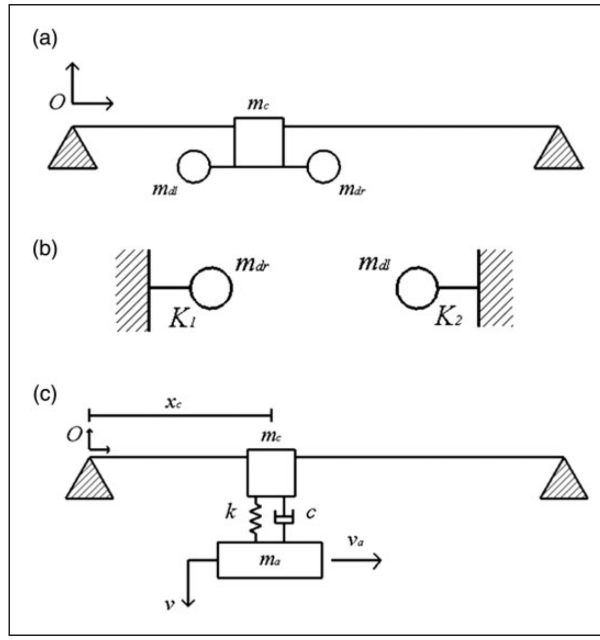

Figure 1. (a) schematic of Stockbridge damper attached to a conductor; (b) schematic of each side of the messenger damper with end masses; (c) schematic of a simply supported beam with a moving mass-spring-damper-mass absorber.

3. Mathematical model

The position vectors for the beam, in-span mass, and the suspended mass are given as

$$\boldsymbol{r_b} = x\boldsymbol{i} + y(x,t)\boldsymbol{j} \tag{1}$$

$$\boldsymbol{r_c} = x_c\boldsymbol{i} + y(x_c,t)\boldsymbol{j} \tag{2}$$

$$\boldsymbol{r_a} = x_c\boldsymbol{i} + v\boldsymbol{j} \tag{3}$$

The velocity vectors are obtained by taking the derivative with respect to time as the following:

$$\dot{\boldsymbol{r}}_{\boldsymbol{b}} = \frac{\partial y(x,t)}{\partial t}\boldsymbol{j} \tag{4}$$

$$\dot{\boldsymbol{r}}_{\boldsymbol{c}} = \frac{\mathrm{d}x_c}{\mathrm{d}t}\boldsymbol{i} + \left(\frac{\partial y(x_c,t)}{\partial t} + \frac{\partial y(x_c,t)}{\partial x_c}\cdot\frac{\mathrm{d}x_c}{\mathrm{d}t}\right)\boldsymbol{j} \tag{5}$$

$$\dot{\boldsymbol{r}}_{\boldsymbol{a}} = \frac{\mathrm{d}x_c}{\mathrm{d}t}\boldsymbol{i} + v_a\boldsymbol{j} \tag{6}$$

where the term $\frac{\mathrm{d}x_c}{\mathrm{d}t}$ is the velocity of absorber v_a.

The kinetic energy of the system can be obtained as

$$\tau = \boldsymbol{T_b} + \boldsymbol{T_c} + \boldsymbol{T_a} \tag{7}$$

where T_b, T_c, and T_a are the kinetic energy of the beam, the in-span mass, and the absorber respectively. Each one of these energies may be expressed as

$$T_b = \frac{1}{2}m\int_0^L \left(\frac{\partial y(x,t)}{\partial t}\right)^2 \mathrm{d}x \tag{8}$$

$$T_c = \frac{1}{2}m_c\left(\left(\frac{\mathrm{d}x_c}{\mathrm{d}t}\right)^2 + \left(\frac{\partial y(x_c,t)}{\partial t} + \frac{\partial y(x_c,t)}{\partial x_c}.\frac{\mathrm{d}x_c}{\mathrm{d}t}\right)^2\right) \tag{9}$$

$$T_a = \frac{1}{2}m_a\left(\frac{\partial y(x_c,t)}{\partial t} + \frac{\partial y(x_c,t)}{\partial x_c}.\frac{\mathrm{d}x_c}{\mathrm{d}t} - \dot{v}\right)^2 \tag{10}$$

The potential energy of the system can be defined as

$$V = \frac{1}{2}EI\int_0^L \left(\frac{\mathrm{d}^2y}{\mathrm{d}x^2}\right)^2 \mathrm{d}x + \frac{1}{2}k(y(x,t)-v)^2 + \frac{1}{2}c\left(\frac{\partial y(x_c,t)}{\partial t} + \frac{\partial y(x_c,t)}{\partial x_c}.\frac{\mathrm{d}x_c}{\mathrm{d}t} - \dot{v}\right)^2 + \frac{1}{2}T\int_0^L \left(\frac{\mathrm{d}y}{\mathrm{d}x}\right)^2 \mathrm{d}x \tag{11}$$

Using these energy expressions along with Hamilton's principle, the governing equations of motion of the system are obtained as

$$EI\frac{d^4y}{\mathrm{d}x^4} + m\frac{\mathrm{d}^2y}{\mathrm{d}t^2} + T\frac{\mathrm{d}^2y}{\mathrm{d}x^2} = F(x,t) - (F_1 + F_2)G(x,t) \tag{12}$$

$$m_a\frac{\mathrm{d}^2v}{\mathrm{d}t^2} - F_2 = 0 \quad x \in (0,L), t > 0 \tag{13}$$

Because the two suspended masses are too small compared to the other masses, and the velocity of the absorber is supposed to be low, the effect of Coriolis acceleration can be neglected, so F_1 and F_2 become

$$F_1 = m_c\left(\frac{\partial^2 y}{\partial t^2}\right) \tag{14}$$

$$F_2 = k(y(x,t)-v) + c\left(\frac{\partial y(x_c,t)}{\partial t} - \dot{v}\right) \tag{15}$$

where y is the displacement of beam, and v is the absolute displacement of m_a.

The $G(x,t)$ is used to define the location profile of the absorber by using the Dirac delta function and Heaviside step function. The function $G(x,t)$ can be expressed as

$$G(x,t) = \begin{cases} g_1, & \textit{fixed absorber} \\ g_2, & \textit{one way moving absorber} \\ g_3, & \textit{two way moving absorber} \\ g_4, & \textit{two way moving absorber} \end{cases} \tag{16}$$

where

$$g_1 = \delta(x - 0.02L) \tag{17a}$$

$$g_2 = \quad \delta(x - V_a t)H\left(0.1\frac{L}{V_a} - t\right) \tag{17b}$$

$$g_3 = \delta(x - V_a t)H\left(0.1\frac{L}{V_a} - t\right) + \delta(x - (.2L - V_a t))H \times \left(t - 0.1\frac{L}{V_a}\right)H\left(0.2\frac{L}{V_a} - t\right) \tag{17c}$$

$$g_4 = g_3 + \delta(x - (0.9L - V_a t))H\left(0.1\frac{L}{V_a} - t\right) + \delta(x - (1.1L - V_a t))H\left(t - 0.1\frac{L}{V_a}\right)H\left(0.2\frac{L}{V_a} - t\right) \tag{17d}$$

where the Heaviside step function is defined as

$$H\left(\frac{L}{V_a} - t\right) = \begin{cases} 1 & t < \frac{L}{V_a} \\ 0 & t \geq \frac{L}{V_a} \end{cases} \tag{18}$$

The boundary conditions and initial conditions are defined as

$$\begin{aligned} y(0,t) = 0; \quad & y(l,t) = 0; \\ \frac{\partial^2 y}{\partial x^2}(0,t) = 0; \quad & \frac{\partial^2 y}{\partial x^2}(L,t) = 0; \end{aligned} \tag{19a}$$

$$y(x,0) = 0: \quad \frac{\partial y}{\partial t} = 0; \tag{19b}$$

$$v(0) = 0; \quad \frac{\partial v}{\partial t} = 0; \tag{19c}$$

The wind excitation force $F(t)$ is given as

$$F(t) = f_0 \sin \omega t \tag{20}$$

where ω is the excitation frequency and f_0 is the drag force, which can be expressed as

$$f_0 = 0.5\rho d C_{\rm d} V_w^2 \tag{21}$$

where d is the diameter of conductor, ρ is the density of fluid (wind), C_d is the drag coefficient, and V_w is the velocity of wind.

The transverse displacement of the beam, which is the solution of the partial differential equation in Equation (12), can be introduced in the form of separation of variable (eigenfunction expansion) as in Samani and Pellicano (2009):

$$y(x,t) = \sum_{r=1}^{\infty} \Phi_r(x) A_r(t) \tag{22}$$

where $A_r(t)$ are unknown functions of time and $\Phi_r(x)$ are the normalized eigenfunctions. Following Samani and Pellicano (2009) and Barry et al. (2014), the eigenfunctions of the bare beam with tension can be obtained as

$$\Phi_r(x) = \sqrt{\frac{2}{ml}} \sin\left(\left(\sqrt{\frac{-T}{2EI} + \sqrt{\frac{T^2}{4(EI)^2} + \frac{m\omega_r^2}{EI}}}\right) x\right) \tag{23}$$

where ω_r represents the natural frequencies of the bare beam and it is given by

$$\omega_r = \left(\frac{\pi}{L}\right)^2 \sqrt{\frac{EI}{m}\left(r^4 + \frac{r^2 T L^2}{\pi^2 EI}\right)} \tag{24}$$

By substituting Equation (22) into Equations (12) and (13) yields

$$\begin{aligned} &EI\sum_{k=1}^{\infty} \frac{d^4\Phi_k}{dx^4} A_k + T\sum_{k=1}^{\infty} \frac{d^2\Phi_k}{dx^2} A_k + m\sum_{k=1}^{\infty} \Phi_k \frac{d^2 A_k}{dt^2} \\ &= -\left[m_c \left(\sum_{k=1}^{\infty} \Phi_k \frac{d^2 A_k}{dt^2}\right)_{x=v_a t} + k\left(\sum_{k=1}^{\infty} \Phi_k A_k - v\right)_{x=v_a t} \right. \\ &\left. + c\left(\sum_{k=1}^{\infty} \Phi_k \dot{A}_k - \dot{v}\right)_{x=v_a t} \right] G(t) + F(x,t) \end{aligned} \tag{25}$$

$$m_a \ddot{v}(t) - k\left(\sum_{k=1}^{\infty} \Phi_k A_k - v\right)_{x=v_a t} - c\left(\sum_{k=1}^{\infty} \Phi_k \dot{A}_k - \dot{v}\right)_{x=v_a t} = 0 \tag{26}$$

Multiplying Equation (25) by $\Phi_i(x)$, integrating over the length and applying the orthogonality conditions yields

$$\begin{aligned} &\ddot{A}_p(t) + M_c\left[\sum_{r=1}^{\infty} \ddot{A}_r(t)\Phi_r(d)\right] \mathrm{D}_p(t) \\ &+ 2\xi\omega_p \dot{A}_p(t) + \omega_p^2 A_p(t) + \{k\left[\sum_{r=1}^{\infty} A_r(t)\Phi_r(d) - v(t)\right] \\ &+ c\left[\sum_{r=1}^{\infty} \dot{A}_r(t)\Phi_r(d) - \dot{v}(t)\right]\} D_p(t) = N_p(t) \end{aligned} \tag{27}$$

$$\begin{aligned} &M_a \ddot{v}(t) - k\left[\sum_{r=1}^{\infty} A_r(t)\Phi_r(d) - v(t)\right] \\ &- c\left[\sum_{r=1}^{\infty} \dot{A}_r(t)\Phi_r(d) - \dot{v}(t)\right] = 0 \end{aligned} \tag{28}$$

where $N_p(t)$ and $D_p(t)$ can be defined as

$$N_p(t) = \int_0^L \Phi_r(x) F(x,t) \mathrm{d}x, \quad r = 1, 2, \ldots \tag{29}$$

$$D_p(t) = \int_0^L \Phi_r(x) G(x,t) \mathrm{d}x, \quad r = 1, 2, \ldots \tag{30}$$

and d is the position of absorber, which is equal to a constant in case of fixed absorber and $v_a t$ in case of moving absorber.

The orthogonality conditions for bare beam subjected to tensile axial force can be expressed as

$$\int_0^L \Phi_s\left[\frac{d^2}{dx^2}\left(EI\frac{d^2\Phi_r(x)}{dx^2}\right) + \frac{d}{dx}\left(T\frac{d\Phi_r(x)}{dx}\right)\right] dx = \omega_r^2 \delta_{rs} \tag{31}$$

$$\int_0^L m\Phi_r(x)\Phi_s(x) \mathrm{d}x, \quad r, s = 1, 2, 3\ldots \tag{32}$$

The performance of the proposed absorber can be evaluated by determining the energy dissipation and is expressed as

$$E = \int_0^{t_1} c\left[\dot{v}(t) - \sum_{r=0}^{\infty} \dot{A}_r(t)\Phi(v_a t)\right]^2 \mathrm{d}t \tag{33}$$

By calculating the energy dissipation for various excitation frequencies and various absorber speeds, the optimum parameters of this absorber can be determined.

The efficiency of the absorber can be obtained as in Samani and Pellicano (2009)

$$\eta = \frac{E}{W} \tag{34}$$

where W is the input energy due to the external force, and it can be expressed as

$$W = \int_0^{t_0} \int_0^L F(x,t)\Phi(x)\dot{A}(t)\mathrm{d}x\,\mathrm{d}t \tag{35}$$

4. Numerical analysis

In the present study, the solution of the ordinary differential equation system, Equations 30 and 31, are obtained numerically using MATLAB®. The simulation includes ten mode expansions and it is based on two different span lengths. The first span length is 4 m which serves for validation of the present model. The second span length, 27.25 m, was used in laboratory testing (Barry et al., 2016) and serves for validation purposes. The value of each parameter in the current study is listed in Tables 1 and 2.

5. Validation

To check for the accuracy of the proposed model, the results of the present simulation are compared to those in the literature. The first case consists of a beam with a fixed absorber and without tension as in Samani and Pellicano (2009). The results are depicted in Figure 2 and show very good agreement.

Table 1. Parameters of beams and applying load.

L (m)	EI (N·m^2)	m (kg/m)	T (N)	ω (rad/s)	f_0 (N/m)
4.00	13959	1.7595	0	0	9.8000
27.25	1602.0	1.6286	27840	125.66	0.4320

Table 2. Parameters of absorber.

L (m)	v_a (m/s)	m_c (kg)	m_a (kg)	k (N/m)	c (N·s/m)
4.00	v_l	0	1.4076	877.92	12.98
27.25	0.1	0.2	4.8000	1356.96	177.00

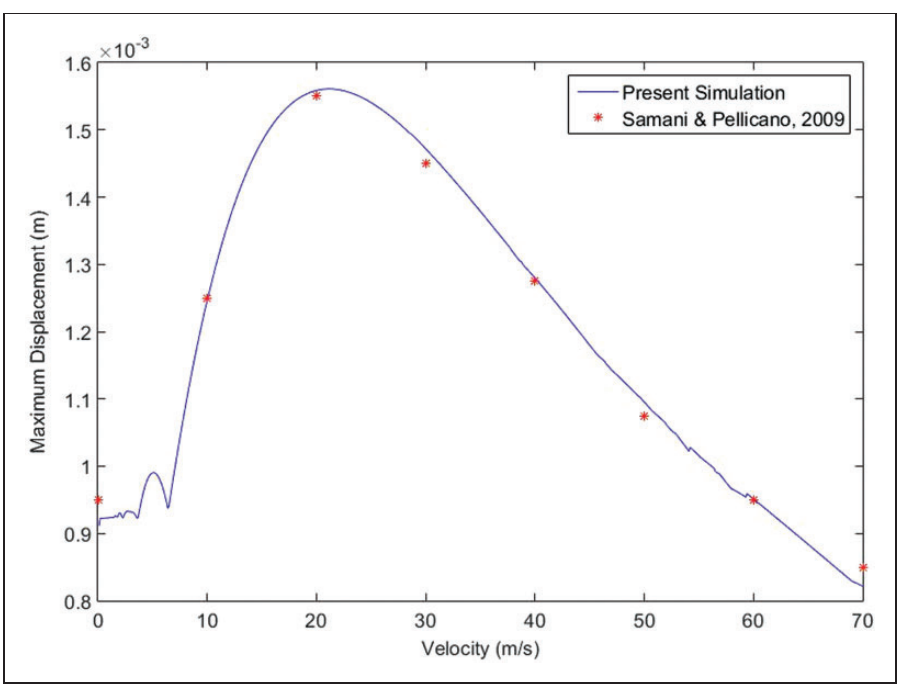

Figure 2. Comparisons of a beam with an attached fixed absorber subjected to moving load.

The second validation of the present model is conducted by comparison with Soares et al. (2010) which consists of a simply supported beam with a moving absorber and no tension. The results are depicted in Figure 3 and show very good agreement.

6. Time response for different types of motion

Figures 4–6 depict the time response for both fixed absorber and moving absorber. The horizontal axis represents the non-dimensional time, which is the time

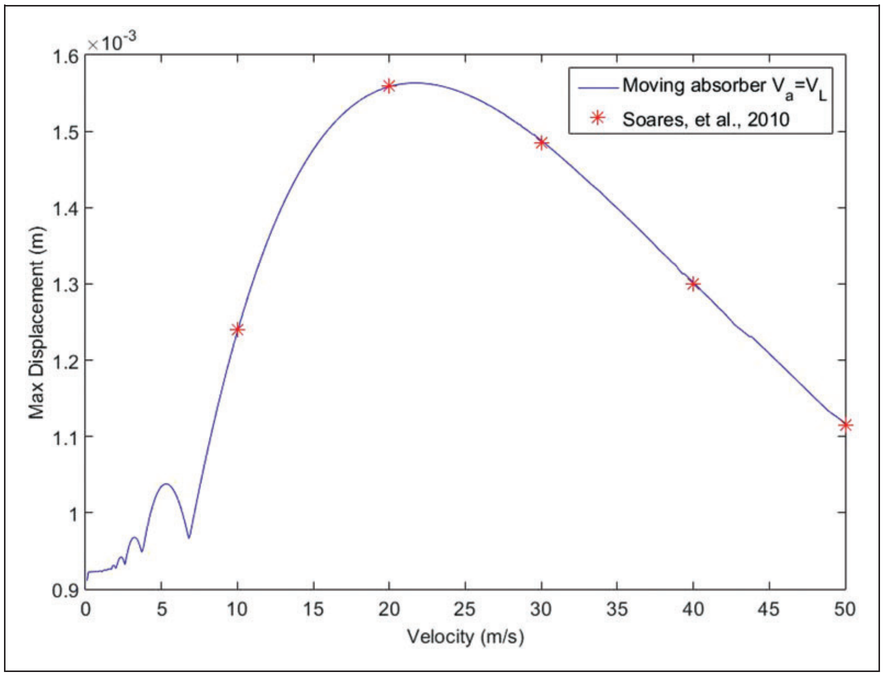

Figure 3. Comparisons of a beam with an attached moving absorber subjected to moving load.

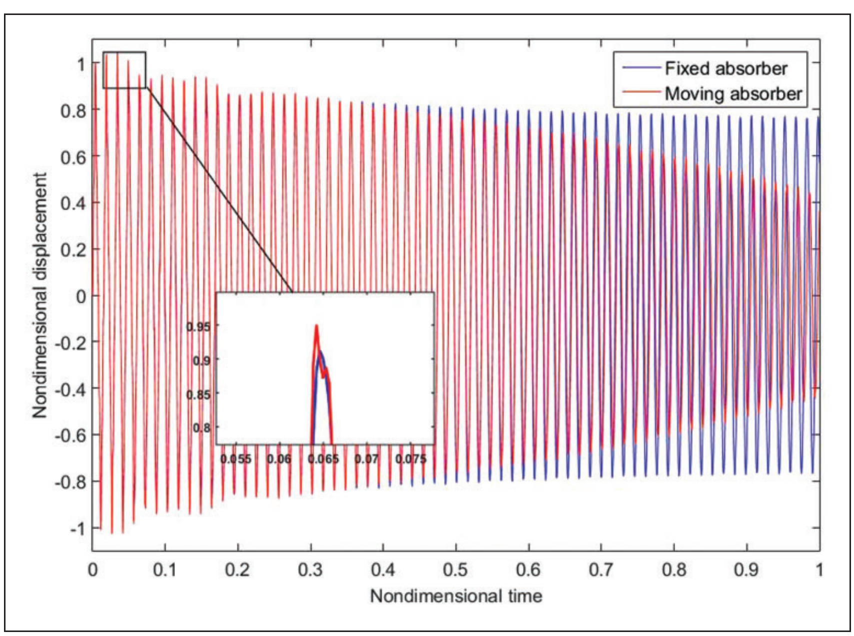

Figure 4. Time response at the mid-span of the conductor for fixed absorber and one way moving absorber. $v_a = 0.1$ m/a; $f = 20$ Hz.

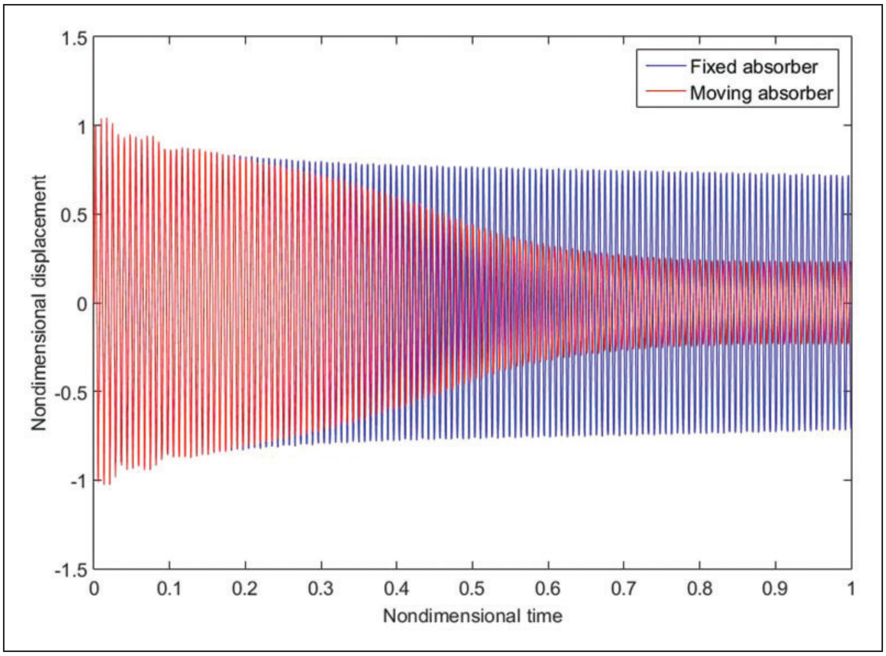

Figure 5. Time response at the mid-span of the conductor for fixed absorber and two way moving absorber. $v_a = 0.1$ m/a; $f = 20$ Hz.

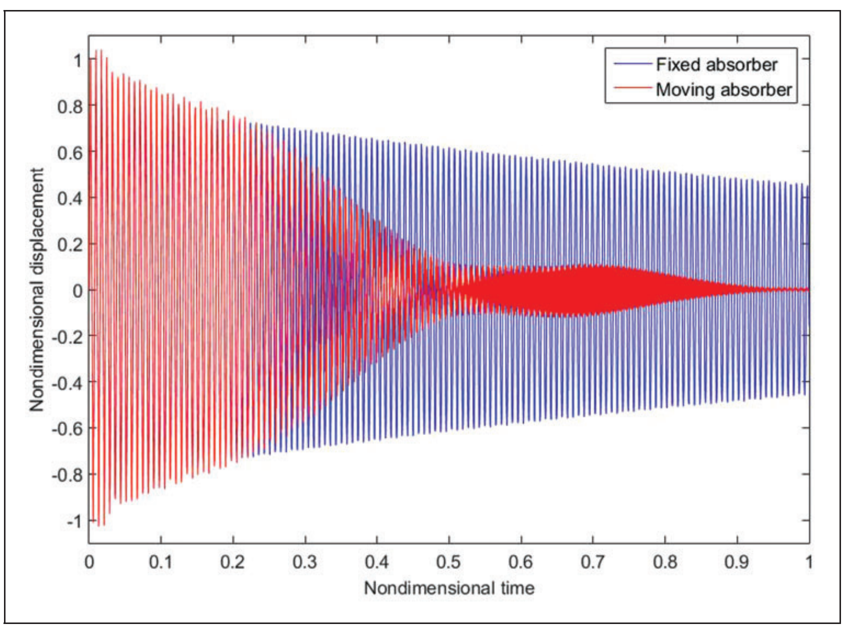

Figure 6. Time response at the mid-span of the conductor for fixed absorber and two two-way moving absorbers.

divided by the required time to complete the absorber movement. The vertical axis represents the non-dimensional displacement, which is the displacement divided by the maximum displacement achieved by the fixed absorber. In the case of the moving absorber, the absorber is considered to move in one-way (only forward) and two-ways (forward and backward). For the one-way moving absorber, it is observed from Figure 4 that the displacement significantly decreases with time compared to the displacement of a fixed absorber. It is also demonstrated that the maximum displacement is slightly higher for the case of a moving absorber at the beginning of the transient response.

In the case of the moving forward and backward absorber, the vibration displacement is reduced significantly as shown in Figure 5. The results in this figure

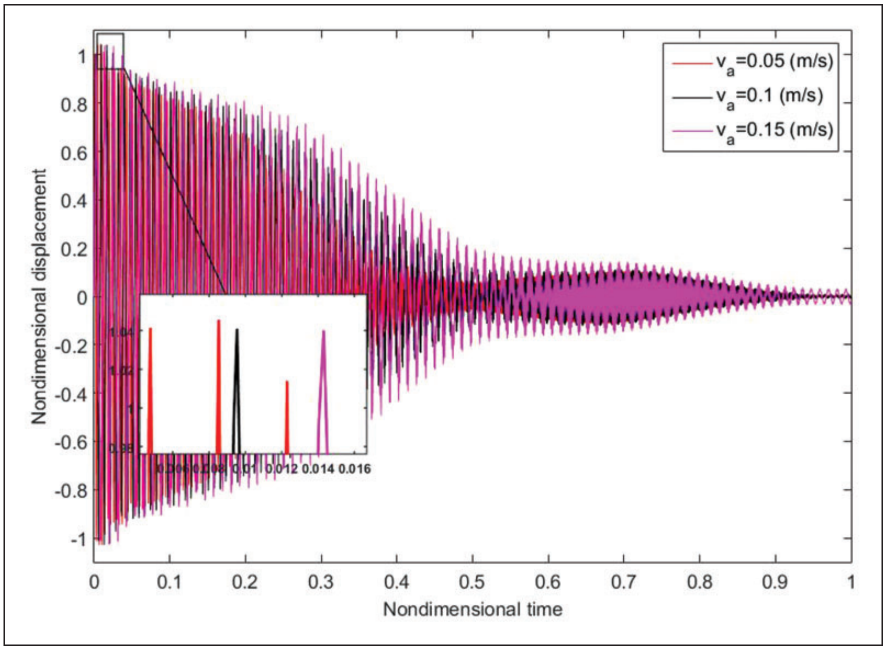

Figure 7. Time response for different absorber velocity.

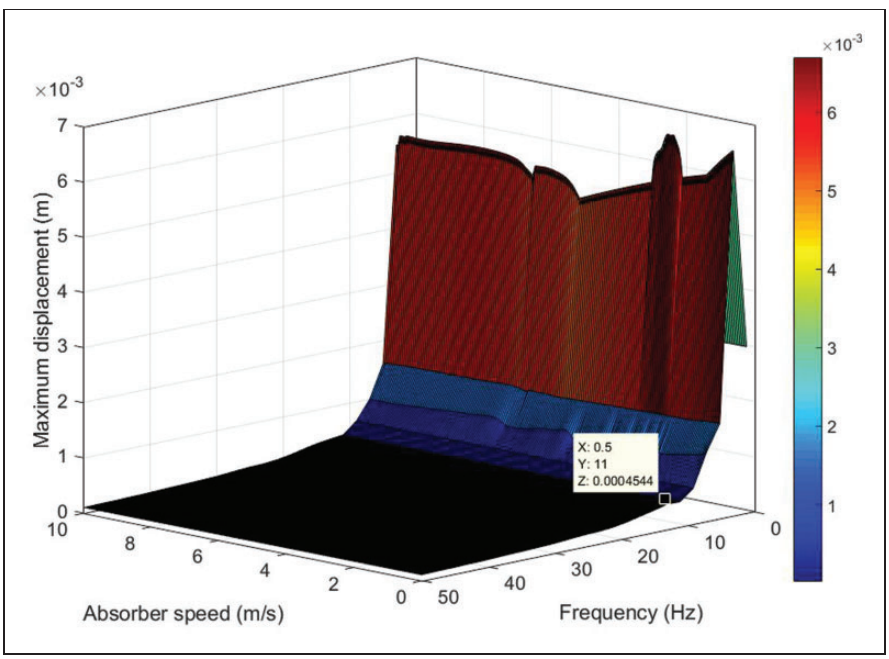

Figure 8. Maximum displacement with variable absorber speeds and forcing frequency.

also indicate that during the time period when the absorber moves forward (half duration), the response is similar to that of the one-way moving absorber.

For a span length of 27.5 m, the results in Figure 6 indicate more reduction in the vibration displacement when an additional absorber is attached at the other end of the conductor. Figure 6 also illustrates that there is a slight increase in the displacement when the absorber starts moving backward, but the vibration displacement is reduced significantly afterwards.

7. The effect of various parameters on the maximum displacement

Figures 7 and 8 show the maximum displacement (i.e., transient response) for variable absorber speeds.

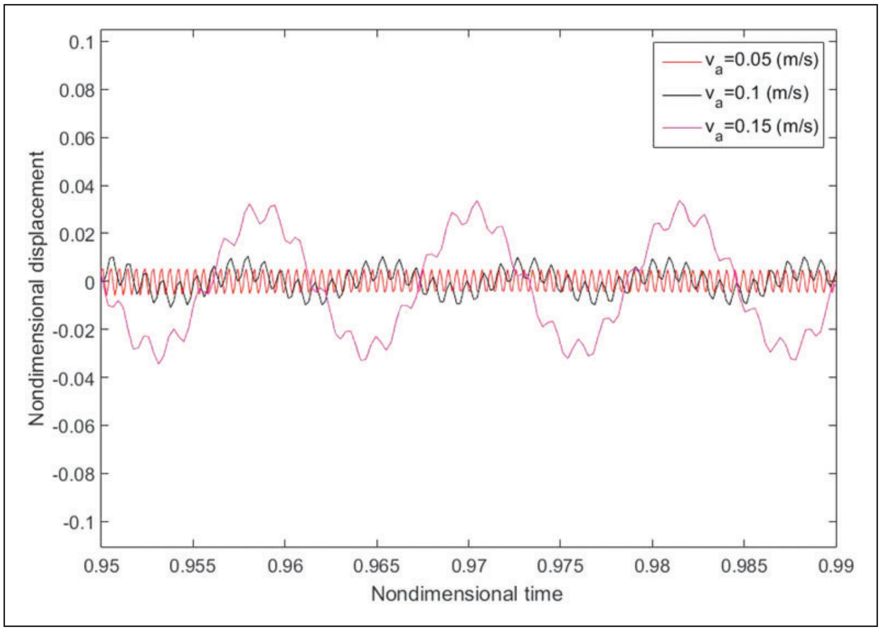

Figure 9. Steady state response for three different absorber speeds.

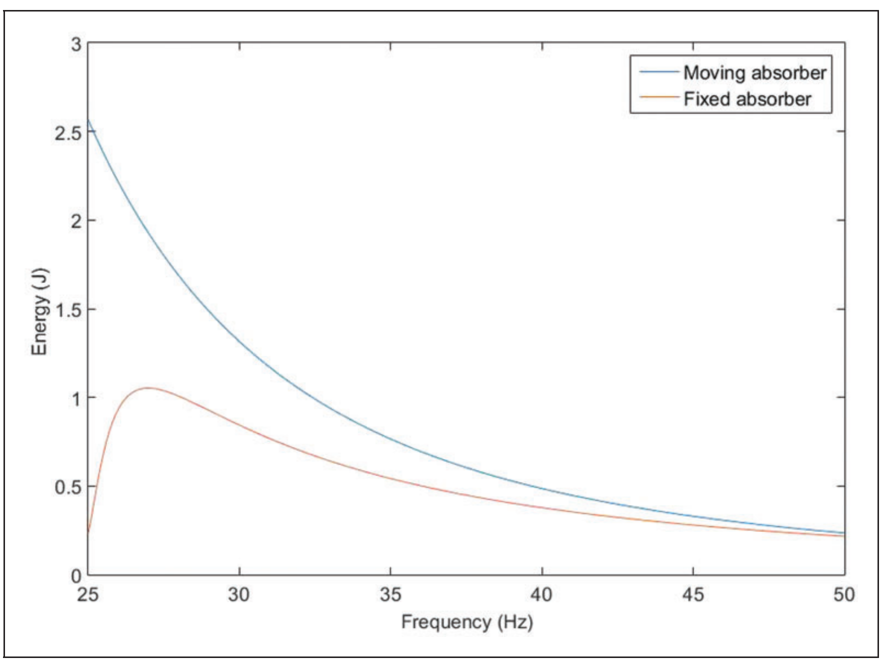

Figure 10. Energy absorbed by absorber for variable frequencies.

The results in Figure 7 show that the maximum displacement changes with the speed of absorber. For further consideration, the maximum displacement is plotted with variable frequencies and absorber speeds as shown in Figure 8. It is observed that the maximum displacement decreases as the frequency increases. The results also indicate that the maximum displacement generally reduces as the speed of the absorber increases for all frequency values. However, near resonance, the maximum displacement fluctuates continuously with absorber speed for frequencies lower than 10 Hz.

Although the results in Figure 8 show that the transient vibration displacement decreases with increasing absorber velocity, the steady state vibration displacement increases with increasing absorber velocity.

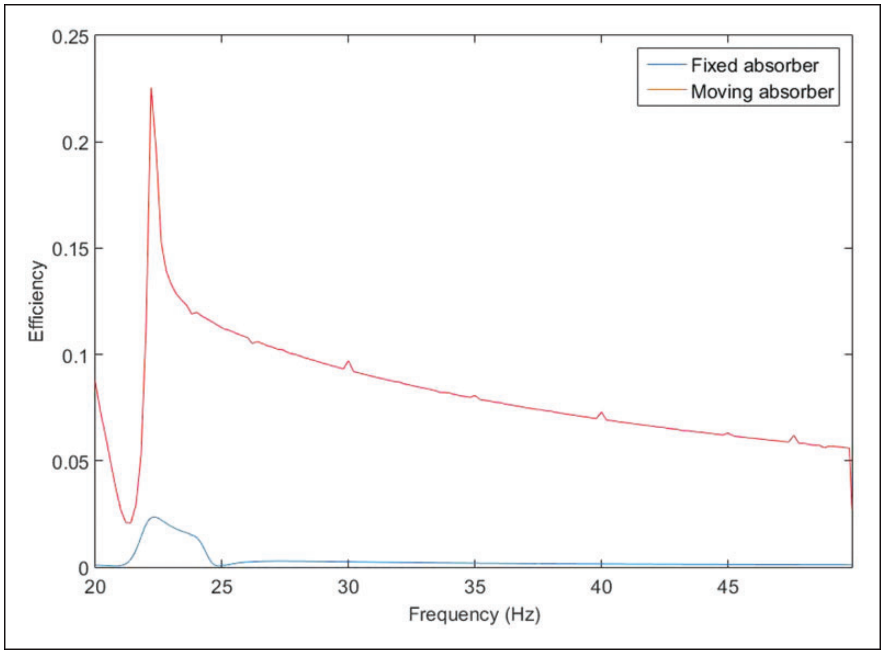

Figure 11. The efficiency of moving and fixed absorber.

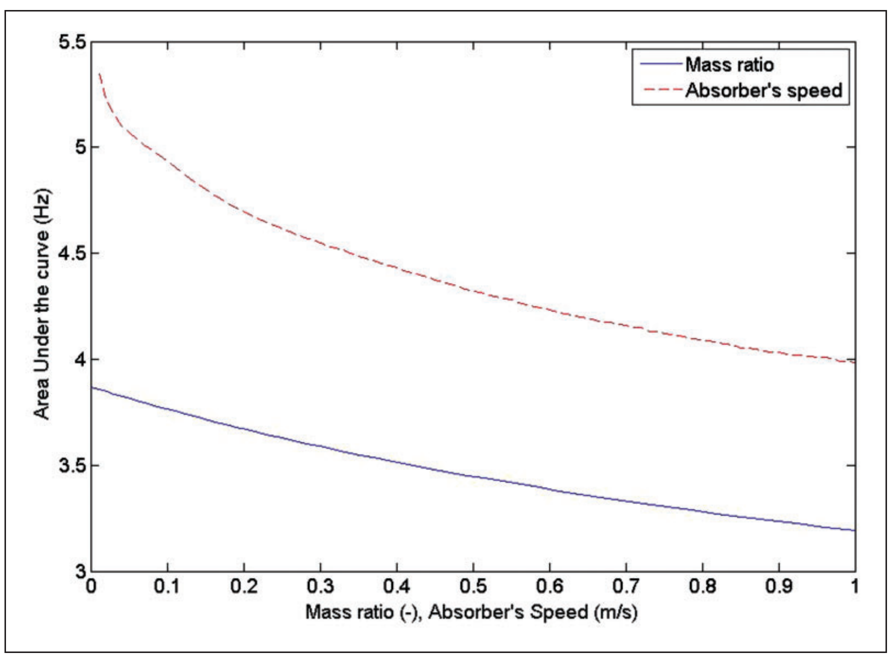

Figure 12. Coverage range of moving absorber with variable absorber speeds and mass ratio.

At the same time, the number of cycles decreases as the velocity of the absorber increases as shown in Figure 9.

8. Performance of moving absorber based on its efficiency

A more reasonable investigation of the performance of the moving absorber can be achieved by calculating the energy dissipation by the absorber and the efficiency.

Figure 10 illustrates the energy absorbed by the absorber for different frequencies. It is observed that the moving damper can absorb more energy for a wider range of frequencies.

The efficiency of both absorbers is depicted in Figure. 11. The results indicate that the efficiency of

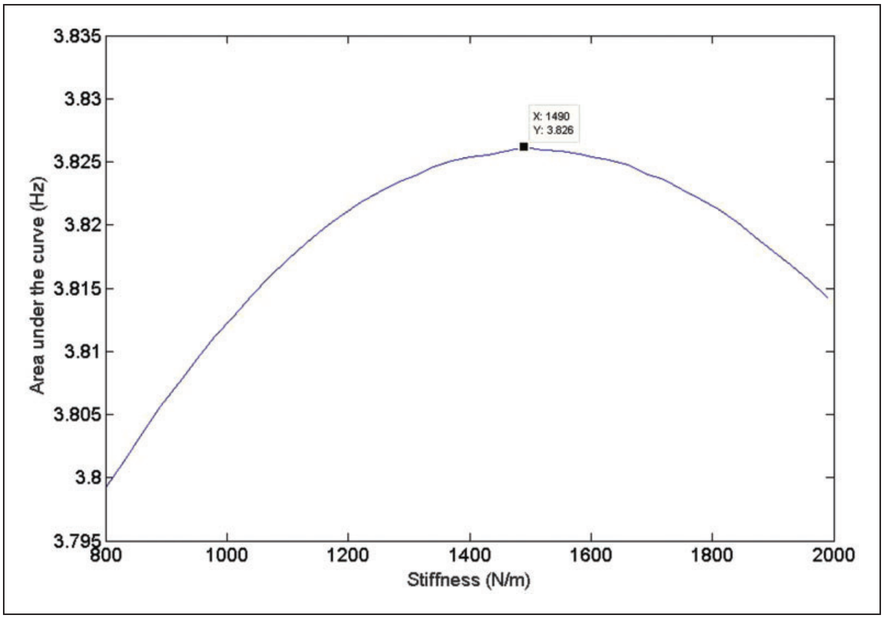

Figure 13. Coverage range of moving absorber with variable spring stiffness. $v_a = 0.6$ m/s.

moving absorber is higher than the fixed absorber. This implies that the area under the efficiency curve is also higher for the moving absorber. Increasing the area under this curve means increasing the coverage range of frequencies thereby enhancing the absorber's performance. Figure 12 depicts the area under the efficiency–frequency curve for variable absorber speeds and mass ratios (i.e., mass ratio is the ratio between the clamped mass to the suspended mass such that the sum of these masses does not exceed 5 kg). The results indicate that the efficiency of the absorber decreases with increasing velocity and increasing suspended mass. Figure 13 shows the area under the efficiency–frequency curve for variable spring stiffness. It indicates that the optimum coverage can be achieved at stiffness value around 1490 N/m.

9. Conclusion

In this paper, a novel Aeolian vibration absorber is proposed. The absorber consists of a mass-spring-damper-mass system and moves along a specific region to cover a wider range of frequencies. Hamilton's principle is used to obtain the governing equations of motion. Numerical simulation is carried out using MATLAB®. Parametric studies are conducted to determine how certain parameters affect the performance of the absorber. Numerical studies indicate that a moving vibration absorber significantly reduces Aeolian vibration for a wider range of frequencies. The results also show that a significant reduction of Aeolian vibration can be achieved by using two absorbers moving forward and backward. It is also observed that the maximum transient vibration displacement decreases with increasing absorber velocity. However, the steady state vibration displacement increases with increasing velocity. The results of the numerical analysis also demonstrate that a moving damper dissipates more energy in a wider range of frequencies than a fixed damper. This is an indication that the moving absorber is more effective than a fixed absorber.

Declaration of Conflicting Interests

The author(s) declared no potential conflicts of interest with respect to the research, authorship, and/or publication of this article.

Funding

The author(s) disclosed receipt of the following financial support for the research, authorship, and/or publication of this article: The authors thank Central Michigan University for providing the fund to support this work.

References

Alkhaldi HS, Abu-Alshaikh IM and Al-Rabadi AN (2013) Vibration control of fractionally-damped beam subjected to a moving vehicle and attached to fractionally-damped multiabsorbers. *Advances in Mathematical Physics* doi:10.1155/2013/232160.

Barry O, Oguamanam D and Lin D (2013) Aeolian vibration of a single conductor with a Stockbridge damper. *IMechE: Part C, Journal of Mechanical Engineering Science* 227(5): 935–945.

Barry O, Oguamanam DCD and Zu JW (2014a) On the dynamic analysis of a beam carrying multiple mass-spring-damper system. *Shock and Vibration*. doi:10.1155/2014/485630.

Barry O, Oguamanam D and Zo J (2014b) Nonlinear vibration of an axially loaded beam carrying multiple mass–spring–damper systems. *Nonlinear Dynamics* 77(4): 1597–1608.

Barry O, Zu JW and Oguamanam DCD (2014) Forced vibration of overhead transmission line: analytical and experimental investigation. *Journal of Vibration and Acoustics* 136(4): 041012.

Barry O, Tanbour E and Dejong B (2015a) *Apparatus and Method to Dampen Aeolian Vibrations and to Inspect Overhead Transmission lLnes*. Mount Pleasant, MI: Central Michigan University, School of Engineering and Technology.

Barry O, Zu J and Oguamanam D (2015b) Analytical and experimental investigation of overhead transmission line vibrations. *Journal of Vibration and Control* 21(14): 2825–2837.

Barry O, Long R and Oguamanam DCD (2016) Simplified Vibration Model and analysis of a single-conductor transmission line with dampers. *Proceedings of the Institution of Mechanical Engineers, Part C: Journal of Mechanical Engineering Science* 0954406216660736.

Chang T, Lin G and Chang E (2006) Vibration analysis of a beam with an internal hinge subjected to a random moving oscillator. *International Journal of Solids and Structures* 43(21): 6398–6412.

EPRI (2006) *Transmission Line Reference Book: Wind Induced Conductor Motion*. Palo Alto, CA: Electrical Power Research Institute.

Gašić V, Zrnić N, Obradović A, et al. (2011) Consideration of moving oscillator problem in dynamic responses of bridge cranes. *FME Transactions* V 39(1): 17–24.

Jaksic V, O'Connor A and Pakrashi V (2014) Damage detection and calibration from beam–moving oscillator interaction employing surface roughness. *Journal of Sound and Vibration* 333(17): 3917–3930.

Kraus M and Hagedorn P (1991) Aeolian vibration: wind energy input evaluated from measurements on an energized transmission lines. *IEEE Transactions on Power Delivery* 6(3): 1264–1270.

Li Z and Ruan Y (2010) Autonomous inspection robot for power transmission lines maintenance while operating on the overhead ground wires. *International Journal of Advanced Robotic Systems* 7(4): 111–116.

Majumder L and Manohar C (2002) A time-domain approachfor damage detection in beam structures using vibration data witha moving oscillator as an excitation source. *Journal of Sound and Vibration* 268(4): 699–716.

Nigol O, Heics RC and Houston HJ (1985) Aeolian vibration of single conductor and its control. *IEEE, Transactions on Power Delivery* 104(11): 3245–3254.

Oguamanam D and Hansen J (1998) Dynamic response of an over head crane system. *Journal of Sound and Vibration* 213(5): 778–895.

Oliveira A and Preire D (1994) Dynamical modeling and analysis of Aeolian vibration of single conductors. *IEEE, Transactions on Power Delivery* 9(3): 1685–1693.

Park J, Lee J and Oh K (2012) An inspection robot for live-line suspension insulator string in 345-kV power lines. *IEEE Transactions on power delivery* 27(2): 632–639.

Pesterev A and Bergman L (2000) An improved series expansion of the solution to the moving oscillator problem. *Journal of Vibration and Acoustics* 122(1): 54–61.

Pesterev AV, Bergman LA, Tan C-A, et al. (2001) On equivalence of the moving mass and moving oscillator problems. In: *Proceedings of the ASME Design Engineering Technical Conference, Pittsburgh, PA*, pp. 1845–1854.

Pesterev AV, Bergman LA, Tan C-A, et al. (2003) On asymptotics of thesolution of the moving oscillator problem. *Journal of Sound and Vibration* 260(3): 519–536.

Rawlins CB (1958) Recent developments in conductor vibration. *Alcoa Technical Paper* Volume 13: 32 pp.

Samani F and Pellicano F (2009) Vibration reduction on beams subjected to moving loads using linear and nonlinear dynamic absorbers. *Journal of Sound and Vibration* 325(4–5): 742–754.

Samani F and Pellicano F (2012) Vibration reduction of beams under successive traveling loads by means of linear and nonlinear dynamic absorbers. *Journal of Sound and Vibration* 331(10): 2272–2290.

Samani F, Pellicano F and Masoumi A (2013) Performances of dynamic vibration absorbers for beams subjected to moving loads. *Nonlinear Dynamics* 73(2013): 1065–1079.

Shafer B (1984) Dynamic modeling of wind induced vibration of over head lines. *International Journal of Non-Linear Mechanics* 19(5): 455–467.

Snowdon J (1965) Vibration of cantilever beams to which dynamic absorbers are attached. *Journal of the Acoustical Society of America* 39(5A): 878–886.

Soares R, Prado Zd and Gonçalves P (2010) On the vibration control of beams using a moving absorber and subjected to moving loads. In: Dvorkin E, Goldschmit and Storti M (eds) *Mecánica Computacional, Volume 29*. Buenos Aires, Argentina: Asociación Argentina de Mecánica Computacional, pp.1829–1840. Available at: http://www.amcaonline.org.ar/ojs/index.php/mc/article/viewFile/3119/3047 (accessed June 2017).

Song Y, Liu Z, Wang H, et al. (2016) Nonlinear analysis of wind-induced vibration of high-speed railway catenary and its influence on pantograph–catenary interaction. *Vehicle System Dynamics* 54(6): 723–747.

Stăncioiu DS, Ouyang H and Mottershead J (2008) Vibration of a beam excited by a moving oscillator considering separation and reattachment. *Journal of Sound and Vibration* 310(4): 1128–1140.

Tompkins JS, Merill LL and Jones BL (1956) Quantitative relationships in conductor vibration using rigid models. *AIEE, Transactions on Power Apparatus and Systems* 75(11): 879–894.

Verma H and Hagerdorn P (2005) Wind induced vibration of long electrical overhead transmission line spans: A modified approach. *Journal of Wind and Structures* 8(2): 89–106.

Wang L, et al. (2010) Development of a practical power transmission line inspection robot based on a novel line walking mechanism. In: *The 2010 IEEE/RSJ International Conference on Intelligent Robots and Systems*, Taipei.

Wu J (2006) Study on the inertia effect of helical spring of the absorber on suppressing the dynamic responses of a beam subjected to a moving load. *Journal of Sound and Vibration* 297(3): 981–999.

Yang B, Tan C and Bergman L (2000) Direct numerical procedure for solution of moving oscillator problem. *Journal of Engineering Mechanics* 126(5): 462–469.

Appendix

Nomenclature

Symbols	Definition	Units
A	The assumed functions of time	s
c	The damping coefficient for damper in absorber	$N.s/m^2$
C_d	The drag coefficient	–
d	The diameter of conductor	m
EI	The stiffness of the beam	$N.m^2$
E	The energy absorption by the absorber	Joule
eff	The effectiveness of absorber	–
$F(x,t)$	The applied axial force	N
f_0	The magnitude of force	N
F_1	Force due to in-span mass	N
F_2	Force due to absorber	N
g_1	The profile function of location for fixed absorber	–
g_2	The profile function of motion for one way absorber	–
g_3	The profile function of motion for two-way absorber	–
g_4	The profile function of motion for two-moving absorber	–
$H(t)$	Heaviside function	–
k	The stiffness of spring in the absorber	N/m
L	The length of the beam	m
m	Mass per unit length for the beam	kg/m
m_a	The mass of absorber	kg
m_c	The mass of mid span	kg
t	Time	s
$\boldsymbol{r_a}$	The position vector of suspended mass	m
$\boldsymbol{r_b}$	The position vector of beam	m
$\boldsymbol{r_c}$	The position vector of in-span mass	m
T	Applied tension on the beam	N
τ	The total kinetic energy	J
T_a	Kinetic energy of the suspended mass	J
T_b	Kinetic energy of the beam	J
T_c	Kinetic energy of the in-span mass	J
u	The net displacement of absorber mass	m
V	The total potential energy of the system	J
v	The absolute displacement of absorber mass	m
v_a	The velocity of absorber	m/s

(continued)

Continued

Symbols	Definition	Units
v_w	The wind velocity	m/s
W	The work done by the beam	J
x	Position on the beam	m
x_c	Position of the absorber	m
y	The lateral displacement of the beam	m
ρ	The density of air	m^3/kg
δ	Dirac function	–
Φ	Displacement function	m
ω_r	Natural frequency	rad/s
ω	Forcing frequency	rad/s